Immunodominance is a poor predictor of vaccine-induced T follicular helper cell quality

Tan HX*[1], Zheng MZM*[1], Wragg K[1], Murdiyarso L[1], Pilapitiya D[1], Kelly A[1], Esterbauer R[1], Gonelli C[1], Wheatley AK†[1], Juno JA†[1]

[1]*Department of Microbiology and Immunology, The University of Melbourne at the Peter Doherty Institute for Infection and Immunity, Melbourne, Victoria 3000, Australia*

These authors contributed equally: Tan HX and Zheng MZM, Wheatley AK and Juno JA

†Correspondence:

Adam K Wheatley, a.wheatley@unimelb.edu.au and Jennifer A Juno, jennifer.juno@unimelb.edu.au

Abstract

Rational engineering of vaccine immunogens to focus B cell responses on potently neutralizing epitopes is a promising approach to improve the potency, breadth and durability of viral vaccines. Such strategies, however, can compromise vaccine immunogenicity through the unintended exclusion of CD4+ T cell epitopes, which are critical for the development of T follicular helper (TFH) cells and to support high affinity antibody production. Using a prototypic influenza HA stem immunogen lacking effective CD4+ T cell help in BL6 mice, we interrogated the minimal requirements for T cell help needed to drive serological responses to vaccination. We find that priming of naïve CD4 T cells is markedly efficient, however the immunodominance of a given CD4 T cell epitope is not predictive of the propensity to provide high quality help to antigen-specific B cells. In the context of soluble antigens, provision of a single MHC class II epitope is sufficient to drive robust germinal centre responses and serum IgG titres. However not all CD4 epitopes provide equivalent levels of B cell help, despite priming comparable numbers of antigen-specific CD4 T cells. Finally, we show multimerizing and arraying antigens on nanoparticle scaffolds unlocks highly subdominant, near-undetectable CD4 T cell helper responses to support a T-dependent antibody response. Our findings emphasize the importance of CD4+ T cell help for programing robust and durable humoral immunity, and provide crucial insights to guide the rational incorporation of favorable T cell epitopes into vaccines.

33 **Introduction**

34 The development of effective vaccines has fundamentally reshaped the ability of human
35 populations to contain and control infectious diseases. While historically vaccines were derived
36 from attenuated or killed whole pathogens, more recent vaccine development efforts have
37 focused upon identification of the most protective "subunits" for inclusion as vaccine
38 immunogens. This was extended during the COVID-19 pandemic, where rational vaccine design
39 was used to engineer the SARS-CoV-2 spike immunogens in protein, mRNA or viral-based
40 vaccines to structurally stabilize[1,2] and/or prevent cleavage[3,4] of the spike trimer. Analogous
41 modifications of the F protein are incorporated into recently approved vaccines for RSV[5].
42 Further efforts to concentrate immunity upon conserved or potently neutralizing domains have
43 seen re-engineering of vaccine immunogens to the level of isolated protein subdomains such as
44 the SARS-CoV-2 RBD[6,7] or stem region of influenza HA[8]. While such small protein targets
45 effectively focus immune recognition by B cells, increasing evidence suggests this might come at
46 a cost to immunogenicity, seen in both pre-clinical models[9,10] and human clinical trials[11,12].

47 Outside of the stochasticity of vaccine delivery, the immunogenicity of vaccine antigens varies,
48 likely reflecting a combination of protein intrinsic factors and host genetics. We and others have
49 identified that a paucity of CD4 helper T cell epitopes is one important factor constraining
50 vaccine immunogenicity[9,10,13,14]. Unlike B cells, whose immunoglobulin receptors scan and
51 engage the near infinite diversity of conformational epitopes on protein surfaces, CD4+ T cells
52 can only recognize linear peptide epitopes in the context of a host MHC-II. This heightened
53 restriction limits the absolute number of T cell epitopes within any given immunogen, with
54 distribution being uneven and individualistic[15]. Reducing the size of a vaccine immunogen
55 therefore has the potential to concomitantly shrink the pool of available CD4+ T cell epitopes,
56 leaving some antigens poorly recognized even in diverse human populations[16-18]. In extreme
57 examples, exemplified by model HA stem[9] or HEL[19] immunogens in genetically inbred
58 C57BL/6 mice, a lack of CD4 T cell epitopes can render immunization immunologically silent.

59 Various strategies have been reported to augment CD4 T cell priming, T follicular helper cell
60 (TFH) differentiation, and subsequent vaccine immunogenicity, but generalized applicability,
61 comparative utility, and mechanisms of action remain unclear. Presentation of vaccine antigens
62 on nanoparticle scaffolds enhances BCR recognition and signaling[20], but can also augment CD4

63 T cell help via epitopes localized within the scaffold[21]. Similarly, covalent coupling of poorly
64 immunogenic proteins to carrier proteins or alternate sources of T cell help can supplement the
65 available antigen-specific CD4 T cell pool[9,22], analogous to the carrier proteins essential for
66 driving antibody responses to pneumococcal carbohydrates in childhood vaccines[23]. However the
67 impacts of epitope specificity or relative immunodominance of polyclonal CD4+ T cell
68 populations upon the capacity to provide help to germinal centre (GC) B cells is poorly
69 understood.

70 Here, we made use of the HA stem-C57BL/6 model[9] to address the features of CD4 T cell
71 immunity that drive potent humoral immune responses to vaccination. We find evidence for a
72 spectrum of epitope-level regulation of GC initiation, with some CD4 T cell specificities unable
73 to support antigen-specific B cell proliferation and IgG production. Critically, epitope
74 immunodominance did not necessarily predict the quality of help provided by antigen-specific
75 CD4 T cells: some immunodominant epitopes exhibited no helper capability, while subdominant
76 responses provided effective help, with even CD4 T cells at near-undetectable levels successfully
77 contributing to GC formation in the context of multimerized antigen. Overall, these data
78 demonstrate that while vaccine immunogenicity is critically dependent on CD4 T cell
79 availability, the capacity to support humoral responses is not universal to all CD4 T cell epitopes,
80 with implications for the rational design of small, engineered vaccine immunogens.

Results

Multimeric display of HA stem antigens on self-assembling ferritin nanoparticles compensates for highly subdominant CD4 help

We previously established primary vaccination of BL/6 mice with a soluble HA stem protein fails to elicit an antigen-specific GC B cell response or production of serum IgG due to a lack of available CD4 T cell epitopes[9]. Presentation of stem on self-assembling ferritin nanoparticles enhances its immunogenicity[24,25] but the source of T cell help in this system is unclear, as BL/6 mice are reported to lack ferritin-specific CD4 T cells[21]. We find that stem-ferritin nanoparticles (Stem-Fe) are robustly immunogenic, eliciting significantly higher stem IgG titres than soluble stem trimers (p=0.0001; Fig1A) and greater numbers of bulk and stem-specific GC B cells (p=0.0001 and p=0.02, respectively; Fig 1B-C, gating in Supplementary Fig 1). Using confocal imaging and flow cytometry, we confirmed the $GL7^{hi}CD38^{lo}$ B cell populations in stem-Fe vaccinated mice reflected *bona fide* GC structures. GL7 expression was correctly localized to GC-like structures within the follicle (Supplementary Fig 2A), and canonical light zone and dark zone GC B cell populations were observed in both full-length HA (HA-FL) and stem-Fe animals (Supplementary Fig 2B), indicative of a T-dependent GC reaction.

Given the lack of identifiable CD4 T cell epitopes within the stem antigen and the limited impact of stem-Fe vaccination on total TFH frequency (Fig 1D), we assessed the magnitude of ferritin-specific responses. We observed limited CD4 T cell responsiveness upon *in vitro* re-stimulation with either stem or ferritin peptide pools (Fig 1E). Similarly, use of a proliferation assay for sensitive detection of any low-frequency populations of stem- or ferritin-specific T cells revealed only sporadic, low-level proliferation when compared to the vehicle control (Fig 1F). To further amplify antigen-specific T cell frequencies, we primed and then boosted mice twice on days 21 and 42. Three out of five Stem-Fe vaccinated animals exhibited clear proliferative responses to the ferritin peptide pool (Fig 2F), suggesting highly subdominant epitopes within ferritin could be the source of T cell help supporting Stem-Fe immunogenicity.

If ferritin-specific CD4 help below the detection limit of conventional T cell assays was responsible for supporting a primary GC reaction, we reasoned that the Stem-Fe antigen should not be immunogenic in transgenic (tg) BL/6 mice that express a single TCR. Conversely, animals with high frequencies of ferritin-specific T cells (i.e. BALB/c mice[21]) should produce superior

111 serological responses. Stem-Fe vaccination of SMARTA tg (BL/6 background), wild-type (WT)
112 BL/6 and WT BALB/c animals demonstrated a striking immunogenicity gradient, with
113 negligible numbers of stem-specific GC B cells (Fig 2A-B) or IgG (Fig 2C) detected in
114 SMARTA mice, while responses in WT BALB/c were more than 20-fold higher compared to
115 WT BL/6 (Fig 2A-C). We confirmed that ferritin-specific CD4 T cells were readily detectible in
116 BALB/c mice by both standard restimulation (Fig 2D) and proliferation assays (Fig 2E),
117 demonstrating that the ferritin core provides substantially more CD4 T cell help in BALB/c
118 versus BL/6 mice.

119 Overall, when stem is arrayed on the surface of a nanoparticle, the low level of ferritin-specific
120 CD4 T cell help available in BL/6 mice becomes sufficient to support a stem-specific GC
121 response that is otherwise absent following soluble stem vaccination.

122 *The TFH repertoire of full-length HA is limited in breadth and dominated by a single epitope*
123 The gradient of Stem-Fe immunogenicity across SMARTA, BL/6 and BALB/c mice strains
124 suggests that availability of CD4 T cell help acts as a rheostat that directly tunes the magnitude
125 of the GC and resultant serological response. While we have established the near-complete lack
126 of CD4 help in stem, the breadth and specificity of epitopes that successfully support the
127 immunogenicity of the full-length HA (HA-FL) protein requires detailed mapping.

128 To maximize the number of TFH for screening, BL/6 mice were infected with a sublethal dose of
129 PR8 influenza virus and mediastinal LN (mLN) which drain the site of infection were collected
130 on day 14. LN cell suspensions were stimulated *in vitro* with a matrix of 20 peptide pools
131 spanning the HA protein (Supplementary Fig 3A), with candidate immunogenic peptides
132 selected by identifying pools that elicited a CD154 response greater than the DMSO control
133 (Supplementary Fig 3B). Individual peptide screening identified 14 potential hits, which we
134 subsequently tested for consistent recognition across multiple animals. Nine peptides elicited
135 CD4 T cell responses in at least 3 of 5 mice, with 4 putative epitopes identified for the
136 $CXCR5^{+}PD\text{-}1^{+}$ CD4 T cell population (enriched for pre-TFH/TFH cells; Fig 3A). $HA_{91\text{-}107}$ was
137 identified as highly immunodominant, with a median of 2.6% of TFH specific for this single
138 peptide. Three other epitopes elicited lower magnitude responses: $HA_{301\text{-}323}$ (two overlapping
139 peptides spanning $HA_{301\text{-}317}$ and $HA_{307\text{-}323}$), $HA_{115\text{-}131}$, and $HA_{523\text{-}539}$ (Fig 3A). A similar hierarchy

140 was observed within the total CD4+ T cell population (Supplementary Fig 3C), with no
141 immunogenic peptides located within the HA-stem domain as expected.

142 To confirm whether these same peptides were immunogenic in the context of vaccination, we
143 intramuscularly immunized mice with 5µg of soluble HA-FL protein in Addavax adjuvant. HA_{91}
144 epitope was again immunodominant, accounting for 74% of the CD154 response to the full HA
145 peptide pool (median of 7.85% $CD154^+$ for HA pool versus 5.76% for HA_{91} peptide)
146 (Supplementary Fig 3D).

147 *Addition of an MHC class II epitope to soluble stem protein rescues stem-specific IgG*

148 Given the wide spectrum of TFH responses capable of modulating serological outcomes, from
149 low-level ferritin-specific help for nanoparticle-driven GCs to the heavy dominance of HA_{91} in
150 the native HA-specific T cell pool, we further sought to clarify the intrinsic "helpfulness" of
151 discrete CD4+ T cell epitopes. We tested whether restoration of a single epitope onto the stem
152 vaccine antigen could prime cognate CD4+ T cells in vivo and thereby improve the stem-specific
153 IgG response. Variants of the trimeric stem immunogen were developed with incorporation of a
154 single peptide epitope sequence adjoined at the C-terminus of the T4 foldon domain (Fig 3B).
155 We produced immunogens incorporating each peptide mapped from HA (HA_{91}, HA_{115}, HA_{301}
156 and HA_{523}) as well as prototypic IA^b-restricted peptides OVA_{323} ('OTII') and LCMV GP_{61}
157 ('SMARTA').

158 WT BL/6 mice were vaccinated with a single 5µg dose of HA-FL, stem, or stem variant antigens
159 formulated in Addavax. On day 14, stem IgG titres were assessed by ELISA and stem-specific
160 GC B cells quantified in the dLN. Only two antigens, stem-HA_{523} and stem-GP_{61}, were capable
161 of eliciting stem-specific IgG and GC B cells at levels above the stem control ($p=0.006$ and
162 $p<0.0001$, respectively; Fig 3C-D). The failure of the immunodominant HA_{91} epitope to rescue
163 the stem response prompted us to examine the biogenesis of the GC response from days 4-14
164 post-vaccination. Stem-HA_{91} vaccinated animals failed to form a stem-specific GC B cell
165 population at any timepoint, while stem-GP_{61}-immunised animals exhibited a robust stem-
166 specific GC response evident from day 6 onwards (Fig 3E). At peak, antigen-specific GC B cell
167 numbers were 33-fold higher in Stem-GP_{61} vaccinated animals compared to HA-FL, with the
168 serological response demonstrating similar durability for both antigens (Fig 3F).

169 *HA_{91}-specific TFH cell fail to populate the germinal centre*

170 Despite HA_{91} dominance in the native CD4+ T cell response to HA-FL vaccination and PR8
171 infection, incorporation of the HA_{91} peptide failed to rescue stem immunogenicity. Possible
172 mechanisms could include a peptide processing defect in the engineered stem immunogen that
173 prevented or reduced naïve CD4 T cell priming by DCs, or alternatively a qualitative defect in
174 TFH differentiation and/or T cell:B cell interactions. To address this, we produced an IA^b/HA_{91}
175 tetramer that facilitated tracking of antigen-specific T cells. In both PR8 infection and HA
176 vaccination, staining of the draining LN with tetramer confirmed the expansion of a prominent
177 $CD44^{hi}$ epitope-specific CD4 T cell population (Supplementary Fig 4A). A similar tetramer
178 successfully identified GP_{61}-specific T cells in dLN following LCMV GP immunization
179 (Supplementary Fig 4A).

180 Using the HA_{91} and GP_{61} tetramers, we compared epitope-specific CD4 T cell numbers and
181 phenotypes at days 4, 5, 6, 10 or 14 post-vaccination with either stem-HA_{91} or stem-GP_{61} (gating
182 in Supplementary Fig 4B). Both antigens readily primed CD4 T cells, evidenced by the
183 expansion of a $tetramer^+$ $CD44^{hi}$ population (Fig 4A) with progressive maturation from a
184 $CD62L^{hi}$ to $CD62L^{lo}$ phenotype (Supplementary Fig 4C). Total numbers of HA_{91}- or GP_{61}-
185 specific T cells in the dLN were comparable, although the stem-HA_{91} antigen primed
186 significantly more $tetramer^+$ cells at day 5 compared to HA-FL protein (Fig 4A). Nevertheless,
187 these populations followed different TFH differentiation trajectories over the subsequent 11
188 days. The small numbers of $CXCR5^{hi}PD\text{-}1^{hi}$ TFH-like GP_{61}-specific cells seen on day 4 became
189 a substantial TFH population by day 6, when median numbers of antigen-specific TFH were 4.2-
190 fold greater for GP_{61} compared to HA_{91} (Fig 4B).

191 Recent work has shown that the identification of TFH based on high CXCR5 and PD-1
192 expression includes cells located both within and adjacent to the GC[26]. Downregulation of
193 surface marker CD90 delineates a population of GC-resident TFH that emerge at day 5 post-
194 immunisation and are dependent on MHCII-expressing B cells for their development and
195 maintenance. Based on CD90 expression, we found significantly higher numbers of GC-resident
196 TFH in stem-GP_{61} compared to stem-HA_{91} vaccinated animals from days 5-10 (Fig 4C). While
197 this was partially driven by the overall greater number of GP_{61}-specific TFH, the dynamics of
198 CD90 downregulation also differed between HA_{91} and GP_{61} TFH populations. From day 5 to 10,

199 the proportion of GP_{61} TFH with a GC-resident phenotype increased from a median of 18.0% to
200 31.4% (Fig 4D). In contrast, the proportion of HA_{91} TFH recruited into the GC declined from
201 6.9% on day 5 to 2.3% on day 10 (Fig 4D). As sustained GC B cell presentation of pMHCII is
202 required to maintain $CD90^{lo}$ TFH populations[26], these data suggested that suboptimal class-II
203 presentation of the HA_{91} peptide by B cells may limit the development of GC-resident TFH.

204 *Broader B cell presentation of HA_{91} supports the Stem-HA_{91} GC response*

205 If differential B cell peptide-MHCII presentation controls the recruitment of ag-specific TFH
206 into the GC, then altering B cell antigen presentation should rescue stem-HA_{91} immunogenicity
207 (Fig 5A). Prior studies have suggested that defects in TFH differentiation can be overcome when
208 DC antigen presentation is extended by boosting a protein immunization with cognate peptide
209 three days later[27]. However, vaccination with 5ug of stem-HA_{91} supplemented with 5ug of free
210 HA_{91} peptide at either day 0 or day 3 failed to rescue stem antibody titres (Fig 5B).

211 We next considered if the small pool of stem-specific naïve B cells may limit the presentation of
212 pMHCII complexes, and contribute to the poor immunogenicity of stem-HA_{91} compared to HA-
213 FL. We therefore immunised mice with 5ug of stem-HA_{91} co-formulated with 5ug of OVA-HA_{91}
214 to increase the potential pool of naïve B cells presenting IA^b/HA_{91}. As controls for the OVA-
215 induced GC response and increased dose of HA_{91} peptide, mice were vaccinated with 5ug of
216 stem-HA_{91} co-formulated with 5ug OVA and an equimolar amount (0.2ug) of free HA_{91}. Only
217 animals vaccinated with stem-HA_{91} and OVA-HA_{91} exhibited stem-specific IgG at day 14 (Fig
218 5B), suggesting that covalent linkage of HA_{91} to an additional B cell antigen was necessary for T
219 cell-B cell interactions that supported a productive stem-specific GC. Both groups exhibited
220 similar HA_{91}-specific T cell frequencies (Fig 5C). While frequencies of bulk HA_{91} TFH were
221 slightly higher in the stem-HA_{91}+OVA-HA_{91} group (median 0.17% of CD4 versus 0.11% for
222 stem-HA_{91}+OVA+HA_{91}), $CD90^{lo}$ GC resident TFH were 1.75-fold more frequent (0.021%
223 versus 0.012%) (Fig 5C).

224 Collectively, these data suggest that the poor performance of the HA_{91} epitope as a sole source of
225 CD4 T cell help is at least partially attributable to a failure to establish or maintain an antigen-
226 specific $CD90^{lo}$ GC-resident TFH population, which can be mitigated by expanding the pool of
227 B cells capable of presenting IA^b/HA_{91} complexes.

228 *Antigen dose differentially impacts CD4 priming and TFH differentiation*

229 If differences in stem-HA_{91} and stem-GP_{61} immunogenicity were driven by pMHCII presentation
230 in the GC, we next asked what the impact would be of reducing GP_{61} peptide availability. To
231 titrate GP_{61} dose without changing the total amount of stem antigen available for B cell uptake,
232 we vaccinated mice with varying doses of the stem-GP_{61} antigen supplemented with unmodified
233 stem, such that the total dose of protein remained 5ug (Fig 6A). Draining lymph nodes were
234 collected at day 6 post-vaccination, the timepoint of maximal GP_{61}-specific T cell expansion and
235 the appearance of stem-specific GC B cells. All immunization doses elicited a similar number of
236 total GP_{61}-specific $CD44^{hi}$ CD4 T cells (Fig 6B), highlighting the marked efficiency of T cell
237 priming by DCs.

238 In contrast, we observed a dose-dependent decrease in GP_{61}-specific TFH differentiation (Fig
239 6B) that paralleled a dose-dependent decline of stem-specific GC B cells (Fig 6C). Accordingly,
240 the number of stem+ GC B cells correlated with the number of ag-specific TFH but not total
241 numbers of ag-specific CD4 T cells (Fig 6D-E), reinforcing that when T cell priming and TFH
242 differentiation are decoupled, GC formation is controlled by TFH availability. Collectively, these
243 data suggest that vaccine dosing sufficient to establish efficient B cell presentation of pMHC to
244 pre-TFH cells is markedly higher than doses required for DC-priming of naïve T cells, and that
245 differences in B cell presentation of HA_{91} and GP_{61} peptides may underpin the differential
246 immunogenicity of stem-HA_{91} and stem-GP_{61} antigens.

247 **Discussion**

248 Engineering vaccine immunogens to reduce inclusion of B cell epitopes with weak or narrow
249 protective capability is an attractive approach for maximizing durable protection against
250 challenging pathogens such as influenza, coronaviruses, HIV, and malaria. While such strategies
251 facilitate highly tailored B cell engagement, increasing evidence suggests that a concomitant loss
252 of CD4 T cell epitopes can hinder overall vaccine immunogenicity *in vivo*. Here, we assessed
253 how CD4 T cell help supports productive GC reactions toward multimerized or soluble protein
254 antigens, and found that T cell epitope specificity, rather than immunodominance, was a
255 determining factor in TFH differentiation and vaccine immunogenicity.

256 Intrinsic protein immunogenicity is likely determined by the complex interplay of multiple
257 factors including B cell precursor frequencies, antigen size, glycosylation, and the ability to elicit
258 an effective CD4 T helper cell response. In a polyclonal system with soluble viral antigens, gross
259 immunogenicity is likely to reflect the totality of available CD4 T cell help, with large antigens
260 generally containing an increased number of CD4 epitopes than small antigens. This is consistent
261 with the observed immunogenicity gradient of stem-ferritin nanoparticles across SMARTA,
262 BL/6 and BALB/c mice; the broad ferritin-specific CD4 T cell pool in BALB/c mice was
263 associated with 10-fold higher stem antibody titres compared to BL/6 animals. This appears to be
264 generally consistent in genetically diverse human cohorts as well: large glycoproteins such as
265 SARS-CoV-2 spike contain sufficient epitopes restricted by a broad array of HLA alleles to
266 support immunogenicity in diverse populations. Small antigens like HA stem, SARS-CoV-2
267 RBD, HIV env or Plasmodium CSP, however, contain reduced numbers of CD4 cell epitopes
268 that begin to restrict the quantity of help available in certain individuals or populations[15-18]. At
269 this point, vaccine immunogens are at higher risk of failure, particularly for pathogens with high
270 antigenic diversity[16].

271 Considering these factors, it becomes essential to understand the minimal requirements for CD4
272 T cell help to support a robust GC reaction. Our data identify distinct scenarios under which
273 vaccination can succeed or fail to generate a serological response. In the context of multimeric
274 arrayed antigens, highly subdominant T cell help becomes sufficient to drive a vaccine-specific
275 serological response. Despite using multiple assays, the frequency of stem- or ferritin-specific
276 CD4 T cells elicited by primary vaccination of BL6 mice appears to be below our limit of

277 detection. Nonetheless, the lack of stem-ferritin immunogenicity in SMARTA transgenic mice
278 and ferritin-specific proliferative responses evident upon repeated boosting clearly support the
279 contribution of low frequency or low affinity antigen-specific T cells to vaccine immunogenicity.
280 Mechanistically, the augmented BCR crosslinking and NF-kB signaling induced by nanoparticle
281 vaccines [20] may potentially reduce the magnitude and/or quality of CD4 T cell help required to
282 initiate a stem-specific GC B cell response.

283 In the context of soluble non-arrayed antigens, we find that a single CD4 epitope is sufficient to
284 support an antigen-specific GC reaction, but perhaps more importantly, find that only some
285 epitopes drive CD4 T cell responses capable of providing suitable B cell help. The potent
286 immunogenicity of the stem-GP_{61} protein clearly demonstrates how even a comparatively
287 restricted CD4 T cell repertoire can support robust GC activity, as the naive repertoire of GP_{61}-
288 specific T cells is heavily biased toward TRAV14/TRAV14D and TRBV13/TRBV31 gene
289 usage[28]. Our data therefore suggest that a highly diverse TFH pool may not be required for
290 vaccine efficacy; rather, the rational selection of a small number of high-quality class II epitopes
291 could be sufficient to support robust humoral immunity.

292 Collectively, our data support the development of GC TFH at an epitope-specific level by two
293 distinct antigen presentation events: naïve T cell priming by DCs which drives
294 immunodominance but not TFH selection, and subsequent T cell-B cell interactions that down
295 select T cell specificities to populate the GC TFH pool. During the first 5 days post-vaccination,
296 the kinetics of T cell expansion were comparable between HA_{91} and GP_{61} epitopes, likely
297 reflecting naïve T cell precursor frequencies which are known to be high for GP_{61} compared to
298 other epitopes such as OTII[28,29]. Interestingly, early DC priming was markedly efficient, as all
299 doses of stem-GP61 antigen tested (0.25ug to 5ug) were saturating for T cell effector frequency,
300 even when they compromised TFH numbers. It is currently unclear whether this is driven by
301 differential antigen processing and presentation in B cells versus DCs, more efficient acquisition
302 by DCs due to immunogen draining patterns in the LN, or a selective threshold imposed by low-
303 frequency CD4 T cell/B cell interactions at the T:B border.

304 It is well known that the major selective event for TFH differentiation and GC residence is
305 recognition of peptide:MHC complexes presented by B cells. However, our data suggest that
306 even in a polyclonal context, there are stark differences in the capacity of epitope-specific T cell

307 populations to provide B cell help. Mechanistically, this appears to be governed by a low
308 propensity of some polyclonal populations (like HA_{91}-reactive T cells) to undergo differentiation
309 into CD90lo GC-resident TFH. Our panel of stem-peptide immunogens identified some
310 'immunocapable' epitopes (GP_{61} and HA_{523}), which support GC responses using the endogenous
311 T cell and B cell repertoire in BL/6 mice. Other epitopes, such as HA_{91}, required manipulation of
312 B:T interactions (e.g. expansion of the peptide-presenting B cell pool) to effectively drive GC.
313 Possible mechanisms underpinning these observations include peptide-intrinsic differences in
314 presentation/processing by B cells (but not DCs) or epitope-specific differences in TCR/MHCII
315 avidity at an aggregate, polyclonal level. The linear relationship between dose of stem-GP_{61} and
316 GP_{61} TFH differentiation suggest the absolute densities of IAb/GP_{61} on the surface of stem-
317 specific B cells dictates a propensity to recruit GP_{61} T cells into the GC, potentially favouring a
318 deterministic role for B cell peptide presentation in controlling TFH composition.

319 Additional study is required to extend these observations into human cohorts. Despite the
320 incredible diversity provided by HLA polymorphism and TCR repertoires, mounting evidence
321 suggests that the human TFH repertoire may also be relatively restricted, with individual
322 epitopes or class II alleles exerting substantial impacts on the outcome of vaccination (Stanford
323 flu paper). Antigens such as HIV env, *Plasmodium* CSP and SARS-CoV-2 RBD frequently
324 contain only 1-2 epitopes that are recognized on an individual level[15-18]. The qualitative
325 differences between HA_{91} and GP_{61} highlight the potential pitfalls of relying on few, endogenous
326 epitopes for consistent vaccine immunogenicity. Further work is required to clarify whether
327 multiple, subdominant epitopes provide additive or synergistic support for GC B cell
328 development. These data also underscore the need to accurately predict the quality of B cell help,
329 rather than just immunogenicity or immunodominance, of any given epitope and responding T
330 cell population to aid vaccine design efforts.

331

332 **Methods**

333 ***Mouse immunizations and infection***

334 C57BL/6, BALB/c, and SMARTA-transgenic (C57BL/6 background) mice were bred in-house
335 under specific pathogen-free conditions in the animal facility at the Peter Doherty Institute of
336 Infection and Immunity, University of Melbourne, Australia. Mouse studies were carried out in
337 accordance with the University of Melbourne Animal Ethics Committee (no. 22954). All mice
338 were female and aged 6 to 12 weeks at the time experiments commenced. A total of 5µg (unless
339 otherwise indicated) of protein, peptide, or nanoparticle were formulated in phosphate buffered
340 saline (PBS) at a 1:1 ratio with Addavax (InvivoGen, cat#INV-vac-adx-10) adjuvant in a total
341 volume of 100µL. Mice were anesthetized by isoflurane inhalation with oxygen flow at 2L/min
342 and isoflurane vaporizer set to 3 (Stinger Anesthetic Machine), prior to 50µl intramuscular
343 injections at the left and right quadriceps using a 29G needle. For influenza infections, mice were
344 anesthetized as above and intranasally infected in a volume of 50µl with a sublethal dose of 50
345 $TCID_{50}$ of A/Puerto Rico/8/34 (PR8). At experimental endpoints, mice were killed using CO_2
346 asphyxiation using a delivery of 50% chamber volume per minute.

347

348 ***Protein expression***

349 Stem and Stem-Ferritin immunogens were prepared in-house, as previously described[9,30]. Briefly,
350 stabilized HA stem proteins were engineered for A/Puerto Rico/08/1934 using methods established
351 previously for the design of Gen6 HA stem in Yassine et al.[24]. Stem-Ferritin nanoparticles were
352 expressed by transient transfection of Expi293F (Life Technologies, Thermo Fisher Scientific)
353 suspension cultures and purified using ion exchange chromatography with HiTrap Q HP column
354 (GE Healthcare) and exclusion chromatography.

355 For stem proteins conjugated to CD4 T cell epitopes, expression constructs substituting the original
356 Avitag for peptide sequences for OTII (ISQAVHAAHAEINEAG), HA_{91}
357 (RSWSYIVETPNSENGIC), HA_{115} (YEELREQLSSVSSFERF), HA_{301}
358 (AINSSLPYQNIHPVTIG), HA_{523} (SMGIYQILAIYSTVASS) and GP_{61}
359 (GLKGPDIYKGVYQFKSVEFD) were synthesized (GeneArt), cloned into mammalian
360 expression vectors and expressed via transient transfection of Expi293 suspension cultures (Life

361 Technologies, Thermo Fisher Scientific). Proteins were purified by polyhistadine-tag affinity
362 chromatography and gel filtration.

363

364 ***Enzyme-linked immunosorbent assay (ELISA)***

365 Blood samples for serum isolation were collected either by submandibular bleed or terminal
366 cardiac puncture bleed using a 26G needle. 96-well MaxiSorp plates (ThermoFisher, cat#
367 3442404) were coated with 2µg/mL recombinant stem protein overnight at 4ºC. Plates were
368 washed with 0.05% (v/v) Tween20 (Sigma, cat# P1379) + PBS and blocked with 1% (v/v) FCS in
369 PBS for 1 hr, room temperature, before incubation with serial dilutions of sera for 2 hr. Plates were
370 washed and horseradish peroxidase-conjugated anti-mouse IgG (1:15 000; Seracare, cat# 5450-
371 0011) was added for 1 hr. After washing, plates were developed with 3,3′,5,5′-
372 Tetramethylbenzidine (TMB; ThermoFisher, cat#SB02), stopped with 0.16M sulfuric acid
373 (Sigma, cat# 84727) and the absorbance measured at 450nm on FLUOstar Omega microplate
374 reader (BMG Labtech). Curves were fitted (four-parameter log regression) and end-point titrations
375 calculated as the reciprocal serum dilution yielding 2x background using GraphPad Prism version
376 10.

377

378 ***Generation of B cell probes and peptide MHC II tetramers***

379 Recombinant biotinylated stem protein biotinylated using BirA (Avidity) and stored at –80°C.
380 Conjugation was performed by sequential addition of streptavidin-PE or -APC (Life Technologies,
381 cat#S866 and S868) or streptavidin-BV711 (BD, cat# 563262). Mouse H2-IAb
382 RSWSYIVETPNSENGI PE-conjugated tetramer (IAb/HA_{91}) was generated by ProImmune.
383 Biotinylated mouse H2-IAb DIYKGVYQFKSV monomer (IAb/GP_{61}; ProImmune) was
384 tetramerized by sequential addition of streptavidin-PE (Life Technologies, cat# S866).

385

386 ***Detection of antigen-specific B and T cells ex vivo***

387 Iliac and inguinal vaccine-draining lymph nodes were passed through a 70µm filter, centrifuged
388 (500*g*, 7 min) and washed with PBS prior to viability staining with live/dead red for 3 min

389 (Invitrogen, cat# L34972). Cells were Fc blocked with anti-CD16/32 antibody (BioLegend, cat#
390 101302) for 10 min and stained with surface antibodies of interest for 30 min at 4ºC. Cells were
391 then washed and fixed with 1% (v/v) formaldehyde (BD, cat# 554655) before acquisition on a
392 BD Symphony or Fortessa flow cytometer. For detection of antigen-specific B cells, PE, APC or
393 BV711 conjugated stem probes were included in the surface staining antibody cocktail. For
394 detection of antigen-specific T cells, single-cell suspensions were pre-incubated at 37ºC with
395 50nM dasatinib (Sigma, cat# SML2589) in 2% (v/v) FCS in PBS containing 1μg/mL anti-TCRβ
396 (BD, cat# 553167). After 30 min, 4μg/mL of IAb/HA_{91} or IAb/GP_{61} tetramers were added for a
397 further 3 hr, before proceeding with viability and surface staining. Data were analyzed using
398 FlowJo (v10.10, BD Biosciences). Data collection and analysis were not performed blind to the
399 conditions of the experiments.

400

401 ***Activation Induced Marker assays***

402 Individual HA, stem (BEI Resources) or ferritin (GenScript) peptides (15-mer with 11 amino acid
403 overlap) were pooled and used to detect antigen-specific CD4+ T cell responses in vitro. LN single
404 cell suspensions were cultured in 96-well round-bottom plates in RPMI-1640 (Thermo Fisher
405 Scientific) with 10% (v/v) FCS and 2% (v/v) penicillin-streptomycin (RF10) media containing
406 20mM A438079 (Santa Cruz, cat# 203788), anti-mouse CD154 antibody and peptide pool of
407 interest (2mg/mL/peptide) or an equivalent volume of DMSO (Sigma, cat# D1435). Following
408 18hr of stimulation, cells were washed in PBS, stained for viability (3 minutes at room
409 temperature) and stained with surface antibodies of interest.

410

411 ***T cell proliferation assay***

412 To generate single-cell suspensions, spleens were passed through a 70μm filter and centrifuged
413 (500xg, 7 min). Red blood cells were lysed using 1x BD PharmLyse (Cat #555899) for 3 min, and
414 the reaction quenched with 1x PBS. Splenic single-cell suspensions were labelled with 2.5mM of
415 CellTrace Violet (CTV; Invitrogen, cat#C34557) for 10 min and washed twice (500xg, 7 min)
416 with RF10. $4x10^5$ CTV-labelled cells were cultured in 96-well round-bottom plates in RF10 with

417 0.5mg/mL HA, stem or ferritin peptide pools, or anti-CD3/CD28 Dynabeads (Gibco, cat #
418 11456D) for 4 days at 37°C, prior to staining for flow cytometric analysis.

419

420 ***Immunofluorescent microscopy***

421 Fresh tissues were snap-frozen in Tissue-Tek O.C.T. compound (Sakura Finetek USA) and stored
422 at -80°C. 7 um sections were cut using the Leica CM3050S cryostat (Leica Biosystems). Prior to
423 staining, sectioned tissues were fixed in cold acetone solution (Sigma) for 10mins, rehydrated with
424 PBS for 10mins, and then blocked in 5% (w/v) bovine serum albumin (Sigma) and 2% (v/v) normal
425 goat serum (Jackson ImmunoResearch). A cocktail of antibodies including GL7 AF488 (clone
426 GL7, BioLegend) and B220 BV421 (clone RA3-6B2, BioLegend) were added for 1 hr at RT.
427 Slides were mounted with ProLong Diamond Antifade Mountant (Life Technologies). Tiled z-
428 stack images at 20x magnification and 1 airy unit were acquired on a LSM780 microscope (ZEISS)
429 and analyzed with Fiji software (REF-Schindelin, 2012, Nat Met).

430

431 ***Statistical analysis***

432 Data are presented as median ± interquartile range. All statistical analysis was performed in Prism
433 10 (GraphPad) using nonparametric statistical tests as indicated (making no assumptions about
434 data normality). $P<0.05$ was considered statistically significant.

435

436 **Acknowledgements**

437 This work was funded by an NHMRC Ideas grant to JAJ. HXT, AKW and JAJ are supported by
438 NHMRC Investigator Grants, and JAJ is supported by the Sylvia and Charles Viertel Senior
439 Medical Research Fellowship. The funders had no role in study design, data collection and
440 analysis, decision to publish or preparation of the manuscript.

441 **Competing interests**

442 The authors declare no competing interests.

443 **Figure Legends**

444 **Figure 1. Nanoparticle display enhances stem immunogenicity in the absence of prominent**
445 **CD4 T cell help**. Mice were vaccinated with 5mg of full-length HA protein (HA-FL), HA-stem
446 protein, or stem-ferritin nanoparticles (Stem-Fe) co-formulated 1:1 with Addavax adjuvant.
447 Serum and draining LN were collected at day 14 post-vaccination. **(A)** Serum endpoint titres of
448 stem-specific IgG (N=10/group). **(B)** Frequency of $GL7^{hi}CD38^{lo}$ GC B cells, **(C)** number of
449 stem-specific GC B cells, or **(D)** frequency of $CXCR5^{hi}PD\text{-}1^{hi}$ TFH in the draining LN
450 (N=10/group). **(E)** Representative staining and frequency of $CD154^{+}$ stem or HA-specific
451 memory CD4 T cells following *in vitro* stimulation. Frequencies are background subtracted
452 based on the DMSO control (N=5/group). **(F)** $CD4^{+}$ T cell proliferation following *in vitro*
453 peptide stimulation with HA, stem or ferritin peptide pools. Splenocytes were harvested from
454 vaccinated mice at day 14, or at day 79 after 3 vaccinations (N=5/group). Lines indicate median
455 and IQR. Statistics assessed by Mann-Whitney test comparing Stem and Stem-Fe groups.
456 *p<0.05, ****p=0.0001

457 **Figure 2. Stem-Fe nanoparticle immunogenicity in SMARTA and BALB/c mice.** Stem-
458 specific **(A)** GC B cell frequencies, **(B)** GC B cell counts or **(C)** IgG titres at day 14 following
459 Stem-Fe vaccination of SMARTA (N=4), WT BL6 (N=10) or BALB/c (N=5) mice. **(D)** Stem- or
460 ferritin-specific $CD4^{+}$ T cell responses in the draining LN of Stem-Fe vaccinated BALB/c mice
461 at day 14 (n=4). **(E)** $CD4^{+}$ T cell proliferation in BALB/c mice following *in vitro* peptide
462 stimulation with DMSO, stem or ferritin peptide pools. Splenocytes were harvested from
463 vaccinated mice at day 14 (N=5/group). Lines indicate median and IQR.

464 **Figure 3. Rescue of stem immunogenicity by genetically fused CD4 T cell epitopes. (A)**
465 Identification of immunogenic peptides following intranasal infection with PR8 virus.
466 Mediastinal LN were collected on day 14 and restimulated in vitro with DMSO, ConA or
467 indicated peptides (N=4-5 mice per peptide). Immunogenic peptides are labelled with the median
468 response and number of responding mice. **(B)** Design of trimeric stem antigens covalently linked
469 to HA-derived peptides or prototypic OVA_{323} and GP_{61} peptides. **(C)** Stem-specific IgG endpoint
470 titres at day 14 post-vaccination with 5ug of HA-FL, stem, or stem-peptide antigens formulated
471 with Addavax (N=7-10 per group). Statistics assessed by Kruskal-Wallis test with Dunn's post-
472 test compared to the stem control. **(D)** Number of stem-specific GC B cells ($GL7^{+}CD38^{lo}$) at day
473 14 post-vaccination (N=4-5 per group). **(E)** Longitudinal tracking of stem-specific GC B cells in
474 the draining LN at days 4, 5, 6, 10 and 14 post-vaccination (N=5 per group). **(F)** Durability of
475 antigen-specific serum IgG following stem-GP_{61} or HA-FL vaccination (N=5 per group).
476 Symbols or lines indicate median with IQR.

477 **Figure 4. Differential GC recruitment of HA_{91} and GP_{61}-specific TFH populations. (A)**
478 Longitudinal tracking of total, **(B)** TFH ($CXCR5^{hi}PD\text{-}1^{hi}$) or **(C)** GC resident TFH ($CD90^{lo}$)
479 antigen-specific $CD4^{+}$ T cell numbers in the draining LN using IA^{b} tetramers. **(D)** Proportion of
480 $tetramer^{+}$ TFH with $CD90^{lo}$ phenotype at days 5, 6 and 10 post-vaccination. Symbols indicate
481 median and IQR (n=5 per group).

482 **Figure 5. Modulation of stemHA$_{91}$ immunogenicity through via altered B cell antigen**
483 **presentation.**
484 **(A)** Overview of immunisation timeline and groups. (**B)** Stem IgG titres at day 14 post-
485 vaccination for groups shown in panel A. N=3-4 per group from either one or two independent
486 experiments. **(C)** Frequencies of total, TFH, or GC TFH HA$_{91}$Tet+ T cells at day 6 post-
487 vaccination with 5ug stem-HA$_{91}$ + 5ug OVA-HA$_{91}$ (light blue) or 5ug stem-HA$_{91}$ + 5ug OVA +
488 0.2ug HA$_{91}$ (dark blue). N=5 per group. Lines indicate median and IQR.

489 **Figure 6. Modulation of stem immunogenicity through via altered B cell antigen**
490 **presentation.**
491 **(A)** Antigen doses for titration of GP$_{61}$ peptide availability. **(B)** Numbers of total and TFH GP$_{61}$
492 Tet+ cells at day 6 post-vaccination (N=5 per group). **(C)** Number of stem-specific GC B cells at
493 day 6 post-vaccination (N=5 per group). Symbols indicate median and IQR. **(D)** Correlation
494 between number of Tet+ TFH or **(E)** total Tet^{+} cells with stem-specific GC B cells. Lymph nodes
495 with no detectible stem-specific B GC B cells were arbitrarily assigned a value of 0.5 (marked
496 with a dashed line) for graphical display. Statistics assessed by Spearman correlation.

497

498 **References**

499 1. Wrapp D, Wang N, Corbett KS, et al. Cryo-EM structure of the 2019-nCoV spike in the prefusion
500 conformation. *Science* 2020; **367**(6483): 1260-3.
501 2. Corbett KS, Edwards DK, Leist SR, et al. SARS-CoV-2 mRNA vaccine design enabled by
502 prototype pathogen preparedness. *Nature* 2020; **586**(7830): 567-71.
503 3. Tian JH, Patel N, Haupt R, et al. SARS-CoV-2 spike glycoprotein vaccine candidate NVX-
504 CoV2373 immunogenicity in baboons and protection in mice. *Nat Commun* 2021; **12**(1): 372.
505 4. Bos R, Rutten L, van der Lubbe JEM, et al. Ad26 vector-based COVID-19 vaccine encoding a
506 prefusion-stabilized SARS-CoV-2 Spike immunogen induces potent humoral and cellular immune
507 responses. *NPJ Vaccines* 2020; **5**: 91.
508 5. Crank MC, Ruckwardt TJ, Chen M, et al. A proof of concept for structure-based vaccine design
509 targeting RSV in humans. *Science* 2019; **365**(6452): 505-9.
510 6. Miranda MC, Kepl E, Navarro MJ, et al. Potent neutralization of SARS-CoV-2 variants by RBD
511 nanoparticle and prefusion-stabilized spike immunogens. *NPJ Vaccines* 2024; **9**(1): 184.
512 7. Nolan TM, Deliyannis G, Griffith M, et al. Interim results from a phase I randomized, placebo-
513 controlled trial of novel SARS-CoV-2 beta variant receptor-binding domain recombinant protein and
514 mRNA vaccines as a 4th dose booster. *EBioMedicine* 2023; **98**: 104878.
515 8. Widge AT, Hofstetter AR, Houser KV, et al. An influenza hemagglutinin stem nanoparticle
516 vaccine induces cross-group 1 neutralizing antibodies in healthy adults. *Sci Transl Med* 2023; **15**(692):
517 eade4790.
518 9. Tan HX, Jegaskanda S, Juno JA, et al. Subdominance and poor intrinsic immunogenicity limit
519 humoral immunity targeting influenza HA stem. *J Clin Invest* 2019; **129**(2): 850-62.
520 10. Tan HX, Juno JA, Lee WS, et al. Immunogenicity of prime-boost protein subunit vaccine
521 strategies against SARS-CoV-2 in mice and macaques. *Nat Commun* 2021; **12**(1): 1403.
522 11. Houser KV, Gaudinski MR, Happe M, et al. Safety and immunogenicity of an HIV-1 prefusion-
523 stabilized envelope trimer (Trimer 4571) vaccine in healthy adults: A first-in-human open-label,
524 randomized, dose-escalation, phase 1 clinical trial. *EClinicalMedicine* 2022; **48**: 101477.
525 12. Hernández-Bernal F, Ricardo-Cobas MC, Martín-Bauta Y, et al. Safety, tolerability, and
526 immunogenicity of a SARS-CoV-2 recombinant spike RBD protein vaccine: A randomised, double-blind,
527 placebo-controlled, phase 1-2 clinical trial (ABDALA Study). *EClinicalMedicine* 2022; **46**: 101383.
528 13. Lee JH, Hu JK, Georgeson E, et al. Modulating the quantity of HIV Env-specific CD4 T cell help
529 promotes rare B cell responses in germinal centers. *J Exp Med* 2021; **218**(2).
530 14. Sarkar S, Kalia V, Murphey-Corb M, Montelaro RC. Detailed analysis of CD4+ Th responses to
531 envelope and Gag proteins of simian immunodeficiency virus reveals an exclusion of broadly reactive Th
532 epitopes from the glycosylated regions of envelope. *J Immunol* 2002; **168**(8): 4001-11.
533 15. Grifoni A, Sidney J, Vita R, et al. SARS-CoV-2 human T cell epitopes: Adaptive immune
534 response against COVID-19. *Cell Host Microbe* 2021; **29**(7): 1076-92.
535 16. Wahl I, Obraztsova AS, Puchan J, et al. Clonal evolution and TCR specificity of the human
536 T(FH) cell response to Plasmodium falciparum CSP. *Sci Immunol* 2022; **7**(72): eabm9644.
537 17. Cohen KW, Fiore-Gartland A, Walsh SR, et al. Trivalent mosaic or consensus HIV immunogens
538 prime humoral and broader cellular immune responses in adults. *J Clin Invest* 2023; **133**(4).
539 18. Juno JA, Tan HX, Lee WS, et al. Humoral and circulating follicular helper T cell responses in
540 recovered patients with COVID-19. *Nat Med* 2020; **26**(9): 1428-34.
541 19. Grewal IS, Moudgil KD, Sercarz EE. Hindrance of binding to class II major histocompatibility
542 complex molecules by a single amino acid residue contiguous to a determinant leads to crypticity of the
543 determinant as well as lack of response to the protein antigen. *Proc Natl Acad Sci U S A* 1995; **92**(5):
544 1779-83.
545 20. Brooks JF, Riggs J, Mueller JL, et al. Molecular basis for potent B cell responses to antigen
546 displayed on particles of viral size. *Nat Immunol* 2023; **24**(10): 1762-77.

547 21. Nelson SA, Richards KA, Glover MA, et al. CD4 T cell epitope abundance in ferritin core
548 potentiates responses to hemagglutinin nanoparticle vaccines. *NPJ Vaccines* 2022; **7**(1): 124.
549 22. Mallajosyula V, Chakraborty S, Sola E, et al. Coupling antigens from multiple subtypes of
550 influenza can broaden antibody and T cell responses. *Science* 2024; **386**(6728): 1389-95.
551 23. Ada G, Isaacs D. Carbohydrate-protein conjugate vaccines. *Clin Microbiol Infect* 2003; **9**(2): 79-
552 85.
553 24. Yassine HM, Boyington JC, McTamney PM, et al. Hemagglutinin-stem nanoparticles generate
554 heterosubtypic influenza protection. *Nat Med* 2015; **21**(9): 1065-70.
555 25. Moin SM, Boyington JC, Boyoglu-Barnum S, et al. Co-immunization with hemagglutinin stem
556 immunogens elicits cross-group neutralizing antibodies and broad protection against influenza A viruses.
557 *Immunity* 2022; **55**(12): 2405-18.e7.
558 26. Yeh CH, Finney J, Okada T, Kurosaki T, Kelsoe G. Primary germinal center-resident T follicular
559 helper cells are a physiologically distinct subset of CXCR5(hi)PD-1(hi) T follicular helper cells. *Immunity*
560 2022; **55**(2): 272-89.e7.
561 27. Deenick EK, Chan A, Ma CS, et al. Follicular helper T cell differentiation requires continuous
562 antigen presentation that is independent of unique B cell signaling. *Immunity* 2010; **33**(2): 241-53.
563 28. Khatun A, Kasmani MY, Zander R, et al. Single-cell lineage mapping of a diverse virus-specific
564 naive CD4 T cell repertoire. *J Exp Med* 2021; **218**(3).
565 29. Jenkins MK, Moon JJ. The role of naive T cell precursor frequency and recruitment in dictating
566 immune response magnitude. *J Immunol* 2012; **188**(9): 4135-40.
567 30. Kelly HG, Tan HX, Juno JA, et al. Self-assembling influenza nanoparticle vaccines drive
568 extended germinal center activity and memory B cell maturation. *JCI Insight* 2020; **5**(10).

569

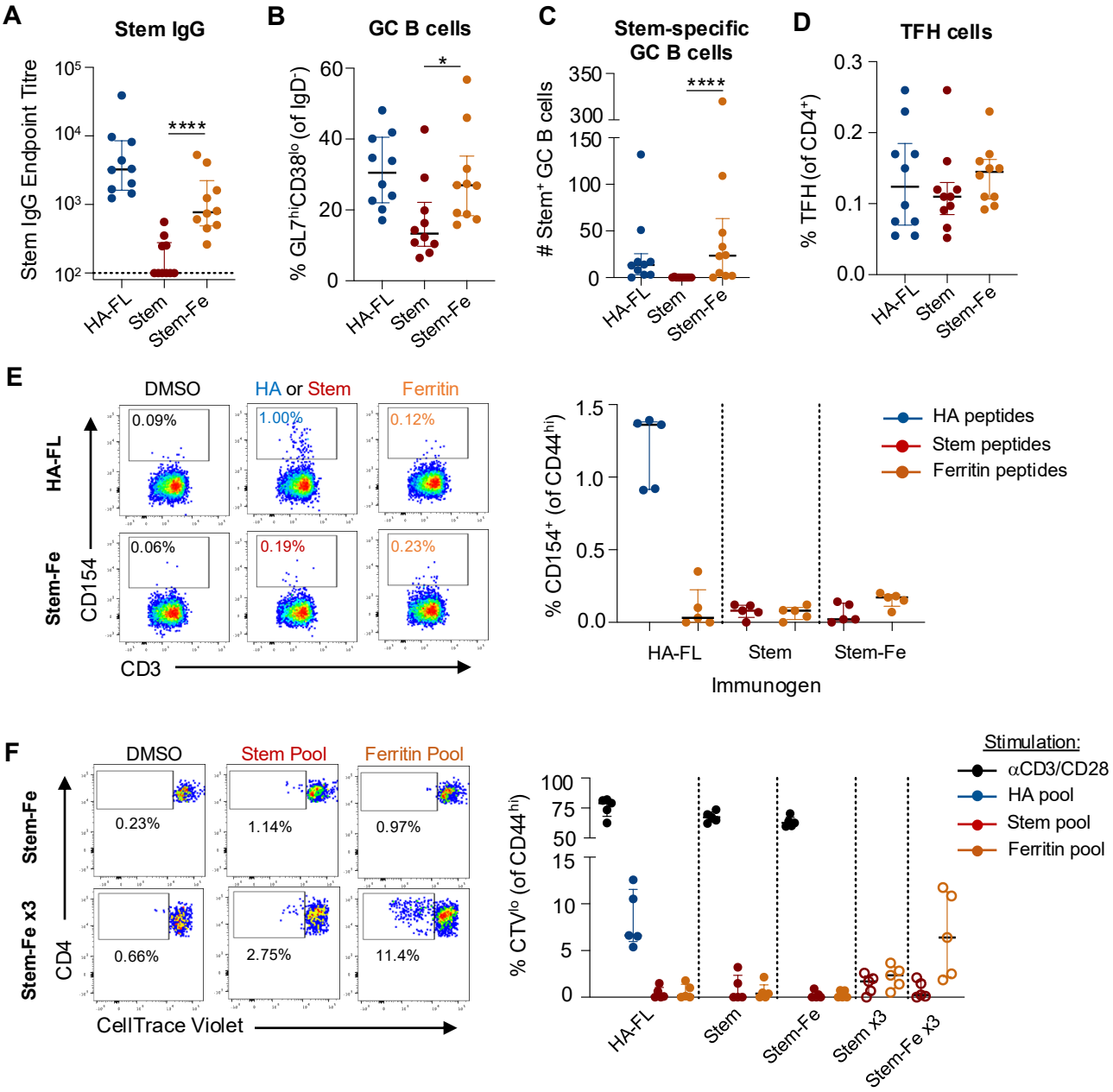

Figure 1. Nanoparticle display enhances stem immunogenicity in the absence of prominent CD4 T cell help. Mice were vaccinated with 5μg of full-length HA protein (HA-FL), HA-stem protein, or stem-ferritin nanoparticles (Stem-Fe) co-formulated 1:1 with Addavax adjuvant. Serum and draining LN were collected at day 14 post-vaccination. **(A)** Serum endpoint titres of stem-specific IgG (N=10/group). **(B)** Frequency of GL7^{hi}CD38^{lo} GC B cells, **(C)** number of stem-specific GC B cells, or **(D)** frequency of CXCR5^{hi}PD-1^{hi} TFH in the draining LN (N=10/group). **(E)** Representative staining and frequency of CD154$^+$ stem or HA-specific memory CD4 T cells following *in vitro* stimulation. Frequencies are background subtracted based on the DMSO control (N=5/group). **(F)** CD4$^+$ T cell proliferation following *in vitro* peptide stimulation with HA, stem or ferritin peptide pools. Splenocytes were harvested from vaccinated mice at day 14, or at day 79 after 3 vaccinations (N=5/group). Lines indicate median and IQR. Statistics assessed by Mann-Whitney test comparing Stem and Stem-Fe groups. *$p<0.05$, ****$p=0.0001$

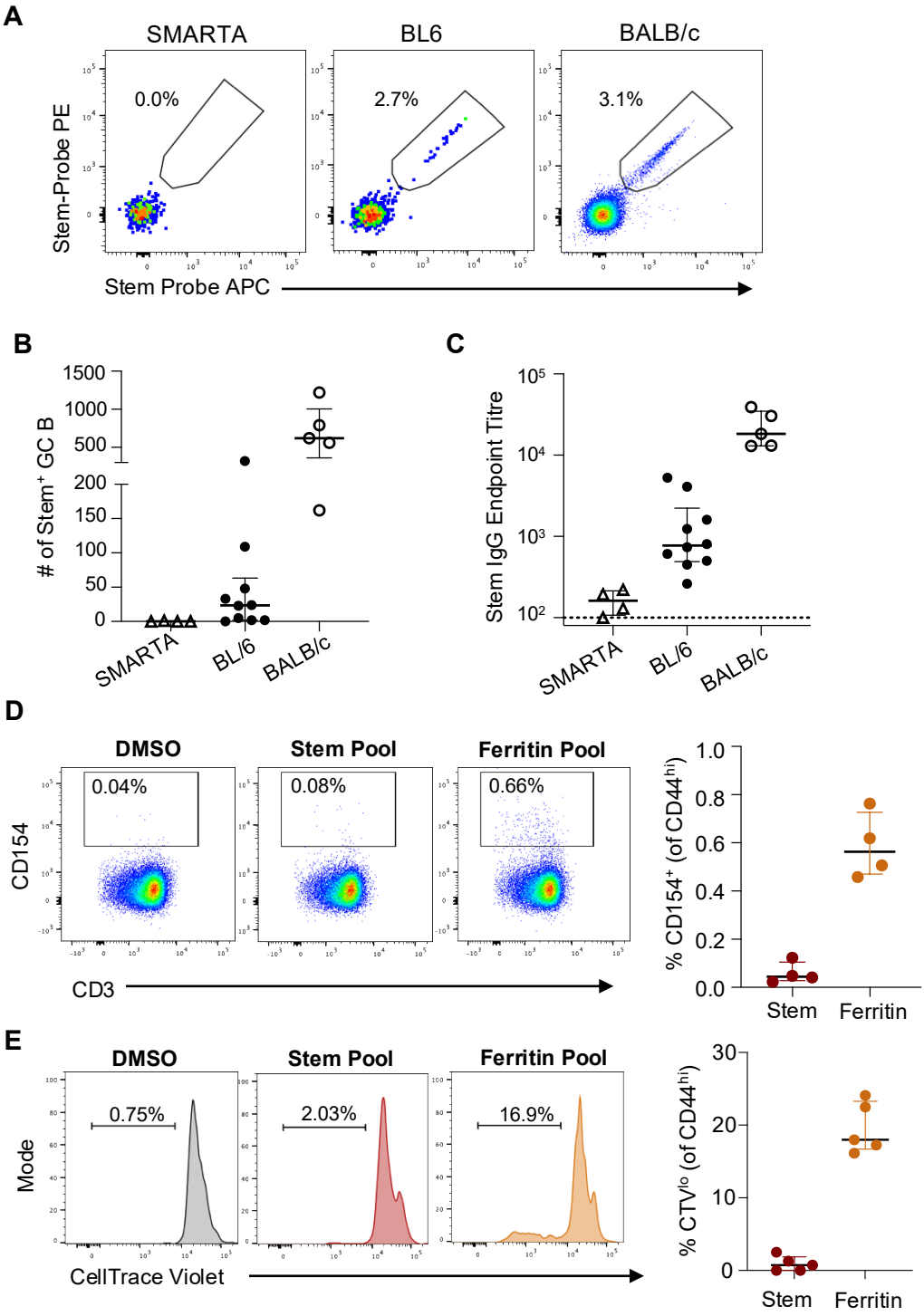

Figure 2. Stem-Fe nanoparticle immunogenicity in SMARTA and BALB/c mice. Stem-specific **(A)** GC B cell frequencies, **(B)** GC B cell counts or **(C)** IgG titres at day 14 following Stem-Fe vaccination of SMARTA (N=4), WT BL6 (N=10) or BALB/c (N=5) mice. **(D)** Stem- or ferritin-specific CD4⁺ T cell responses in the draining LN of Stem-Fe vaccinated BALB/c mice at day 14 (n=4). **(E)** CD4⁺ T cell proliferation in BALB/c mice following *in vitro* peptide stimulation with DMSO, stem or ferritin peptide pools. Splenocytes were harvested from vaccinated mice at day 14 (N=5/group). Lines indicate median and IQR.

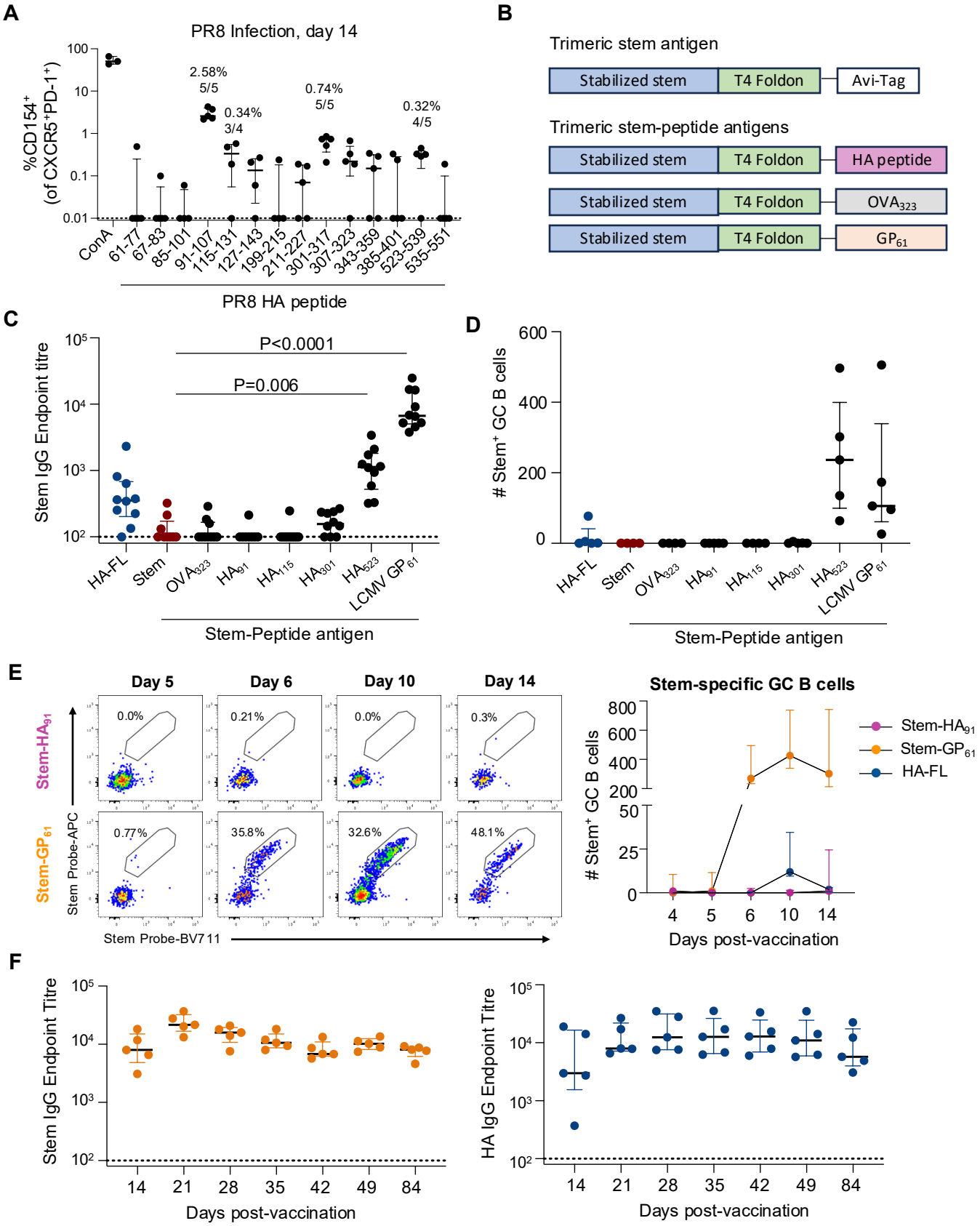

Figure 3. Rescue of stem immunogenicity by genetically fused CD4 T cell epitopes. (A) Identification of immunogenic peptides following intranasal infection with PR8 virus. Mediastinal LN were collected on day 14 and restimulated in vitro with DMSO, ConA or indicated peptides (N=4-5 mice per peptide). Immunogenic peptides are labelled with the median response and number of responding mice. **(B)** Design of trimeric stem antigens covalently linked to HA-derived peptides or prototypic OVA_{323} and GP_{61} peptides. **(C)** Stem-specific IgG endpoint titres at day 14 post-vaccination with 5ug of HA-FL, stem, or stem-peptide antigens formulated with Addavax (N=7-10 per group). Statistics assessed by Kruskal-Wallis test with Dunn's post-test compared to the stem control. **(D)** Number of stem-specific GC B cells ($GL7^+CD38^{lo}$) at day 14 post-vaccination (N=4-5 per group). **(E)** Longitudinal tracking of stem-specific GC B cells in the draining LN at days 4, 5, 6, 10 and 14 post-vaccination (N=5 per group). **(F)** Durability of antigen-specific serum IgG following stem-GP_{61} or HA-FL vaccination (N=5 per group). Symbols or lines indicate median with IQR.

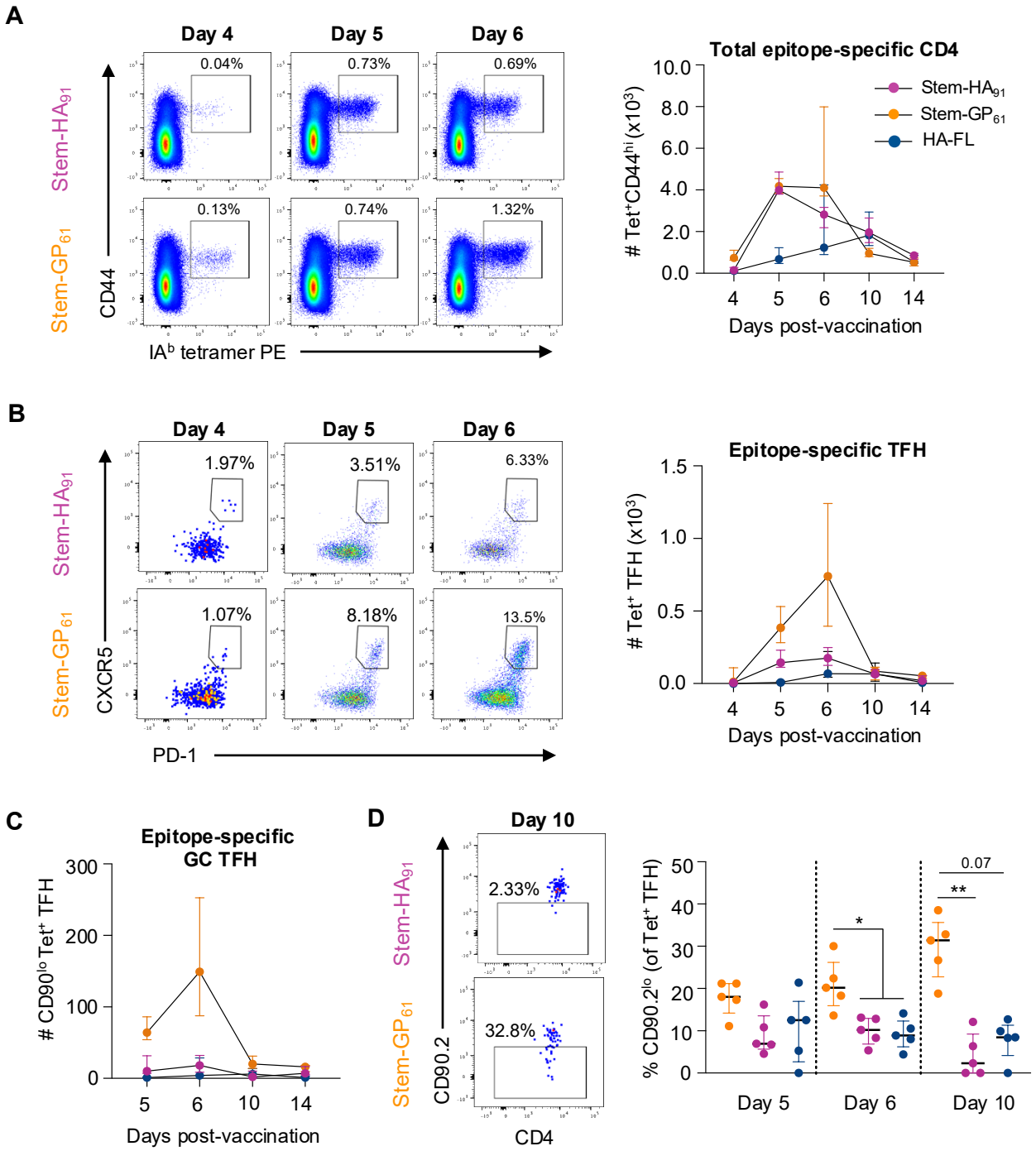

Figure 4. Differential GC recruitment of HA_{91} and GP_{61}-specific TFH populations. (A) Longitudinal tracking of total, **(B)** TFH ($CXCR5^{hi}PD\text{-}1^{hi}$) or **(C)** GC resident TFH ($CD90^{lo}$) antigen-specific $CD4^+$ T cell numbers in the draining LN using IA^b tetramers. **(D)** Proportion of $tetramer^+$ TFH with $CD90^{lo}$ phenotype at days 5, 6 and 10 post-vaccination. Symbols indicate median and IQR (n=5 per group).

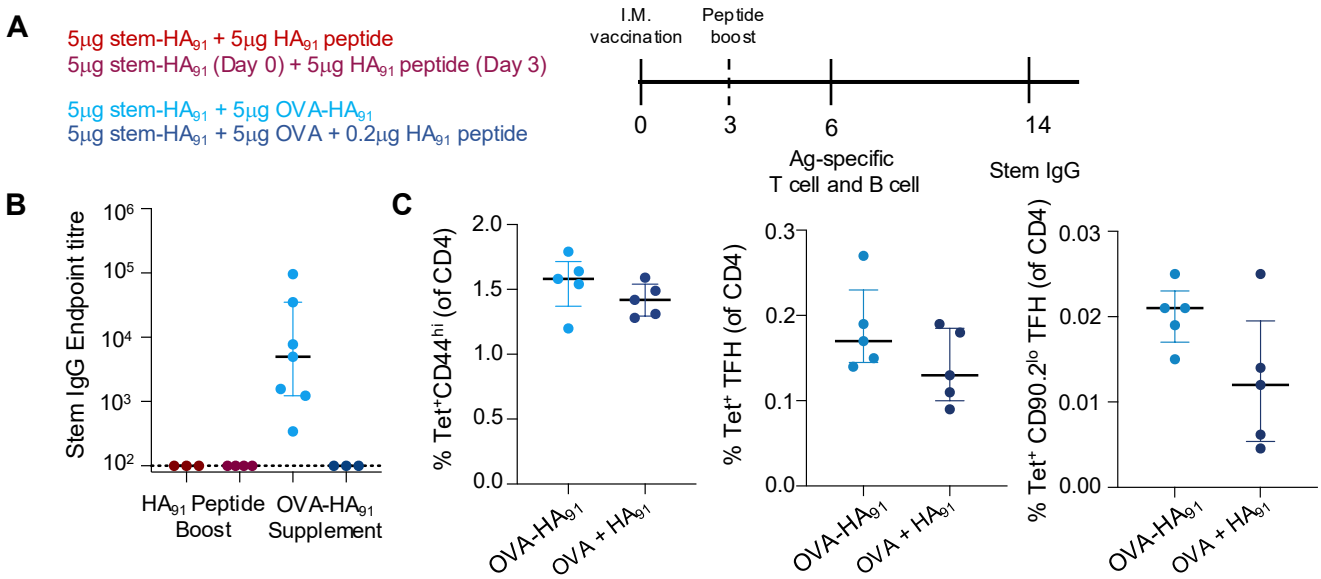

Figure 5. Modulation of stemHA$_{91}$ immunogenicity through via altered B cell antigen presentation. **(A)** Overview of immunisation timeline and groups. (**B)** Stem IgG titres at day 14 post-vaccination for groups shown in panel A. N=3-4 per group from either one or two independent experiments. **(C)** Frequencies of total, TFH, or GC TFH HA$_{91}$Tet+ T cells at day 6 post-vaccination with 5ug stem-HA$_{91}$ + 5ug OVA-HA$_{91}$ (light blue) or 5ug stem-HA$_{91}$ + 5ug OVA + 0.2ug HA$_{91}$ (dark blue). N=5 per group. Lines indicate median and IQR.

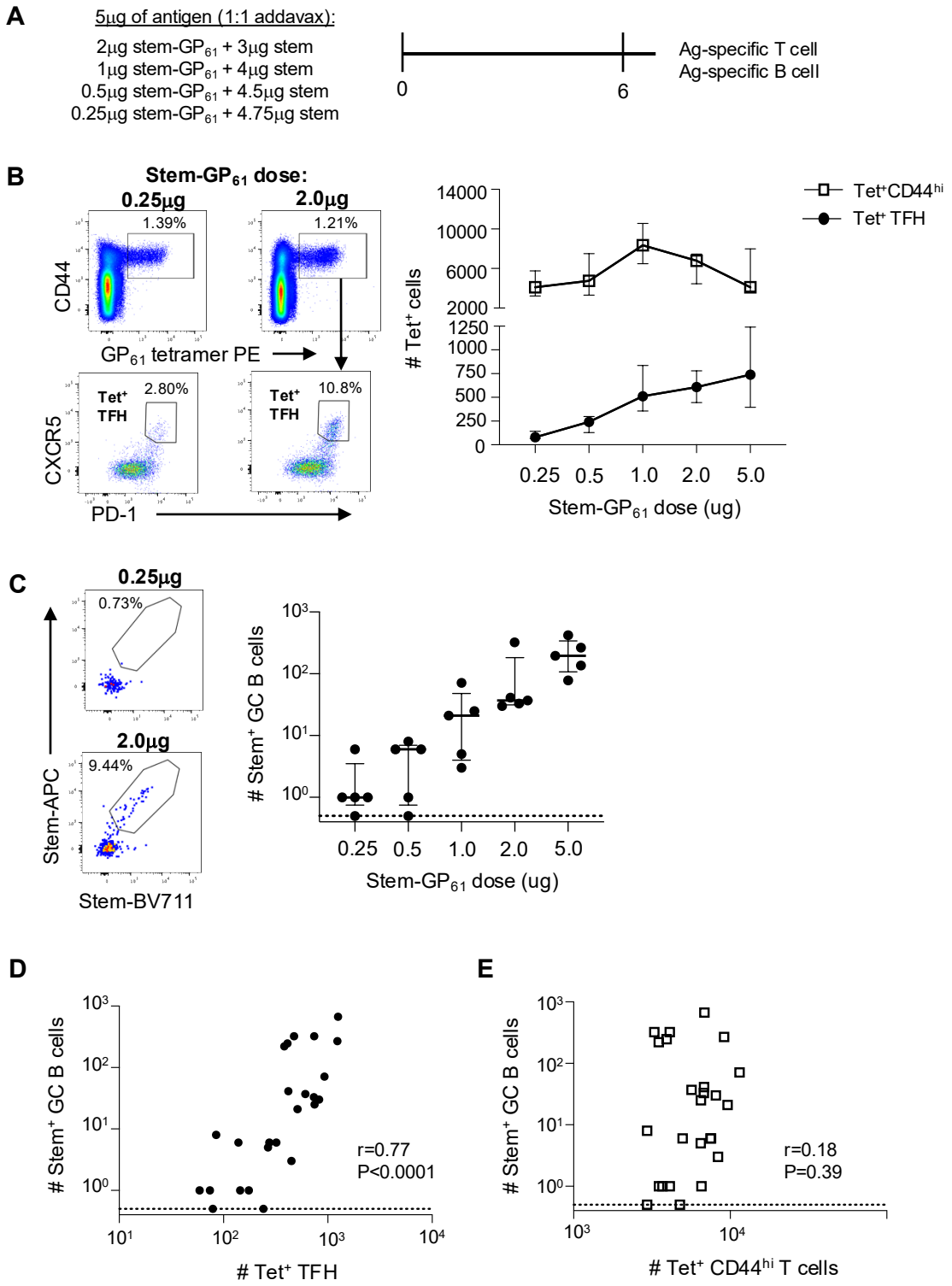

Figure 6. Modulation of stem immunogenicity through via altered B cell antigen presentation.
(A) Antigen doses for titration of GP_{61} peptide availability. **(B)** Numbers of total and TFH GP_{61} Tet+ cells at day 6 post-vaccination (N=5 per group). **(C)** Number of stem-specific GC B cells at day 6 post-vaccination (N=5 per group). Symbols indicate median and IQR. **(D)** Correlation between number of Tet+ TFH or **(E)** total Tet^+ cells with stem-specific GC B cells. Lymph nodes with no detectible stem-specific B GC B cells were arbitrarily assigned a value of 0.5 (marked with a dashed line) for graphical display. Statistics assessed by Spearman correlation.

Supplementary Figures

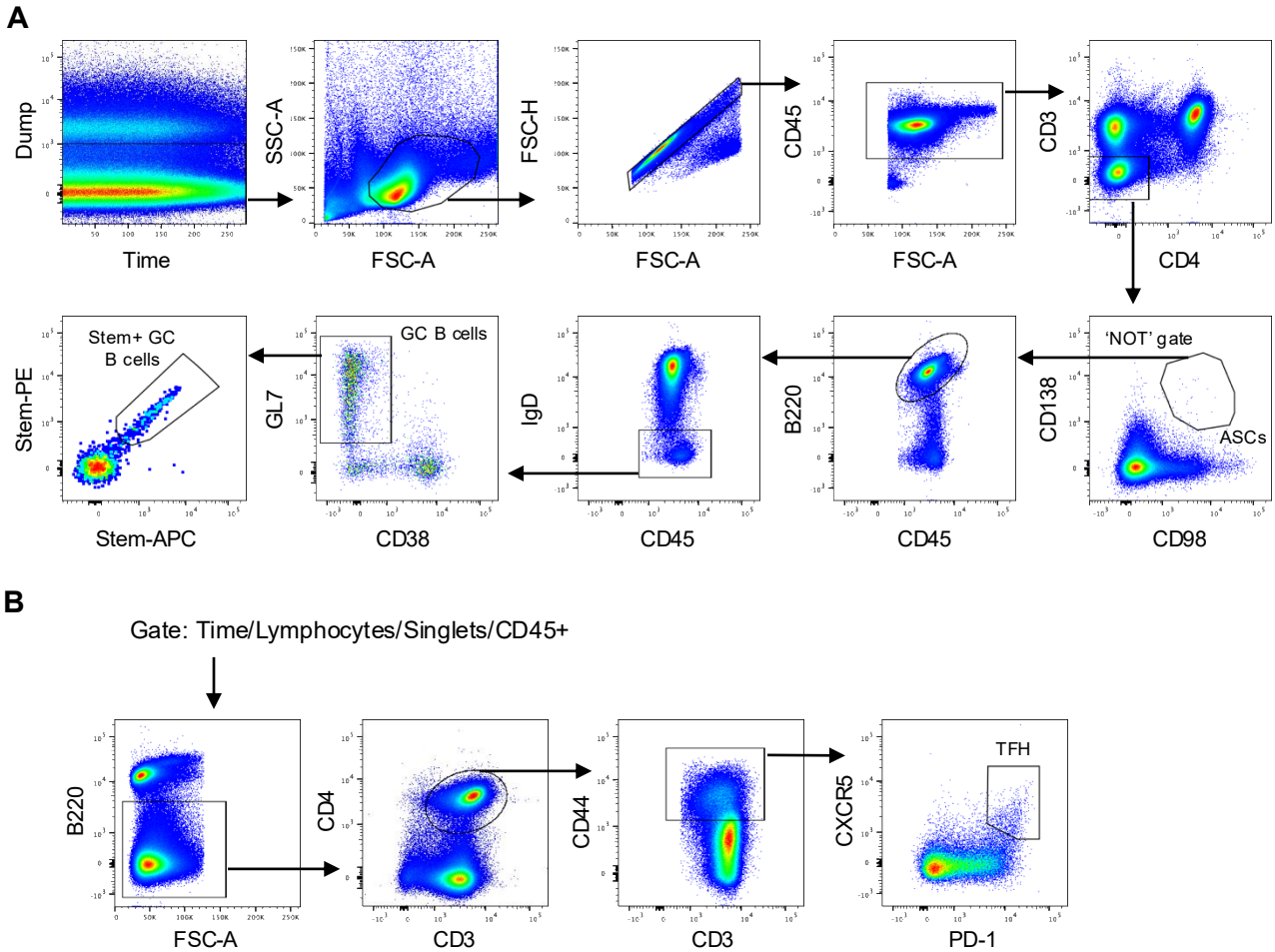

Supplementary Figure 1. Gating strategy for GC B cell and TFH populations.
(A) Lymphocyte populations are gated through a Dump (F4/80 and live/dead) vs Time plot, then identified by forward and side scatter, with exclusion of doublets (FSC-A vs FSC-H) and selection of CD45+ cells. Antibody secreting cells are defined as CD3-CD4- cells that co-express CD138 and CD98. Class-switched B cells are defined as non-ASCs that are B220+ and IgD-. Germinal centre B cells are gated as GL7+CD38lo, and antigen specificity determined by staining with recombinant protein tetramers. **(B)** CD4+ T cells are identified as B220- and CD3+CD4+. Antigen-experienced cells are gated as CD44hi, and TFH are defined as CXCR5+PD-1+ cells.

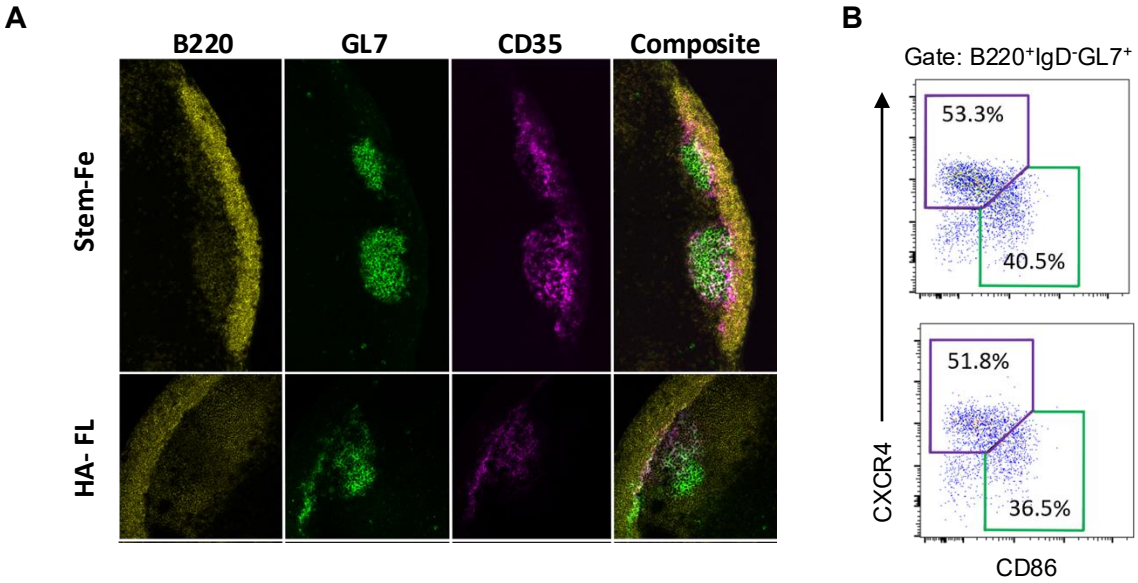

Supplementary Figure 2. Germinal centre morphology following stem-Fe vaccination. (A) Confocal imaging of vaccine draining lymph nodes showing localisation of B220^{+} B cells (yellow), GL7^{+} GC B cells (green), and CD35+ follicular dendritic cells (magenta). (B) Identification of light zone (CXCR4^{lo}CD86^{hi}) and dark zone (CXCR4^{hi}CD86^{lo}) GC B cells in stem-Fe (top) or HA-FL (bottom) vaccinated animals. Data are representative of 5 individual animals in each group.

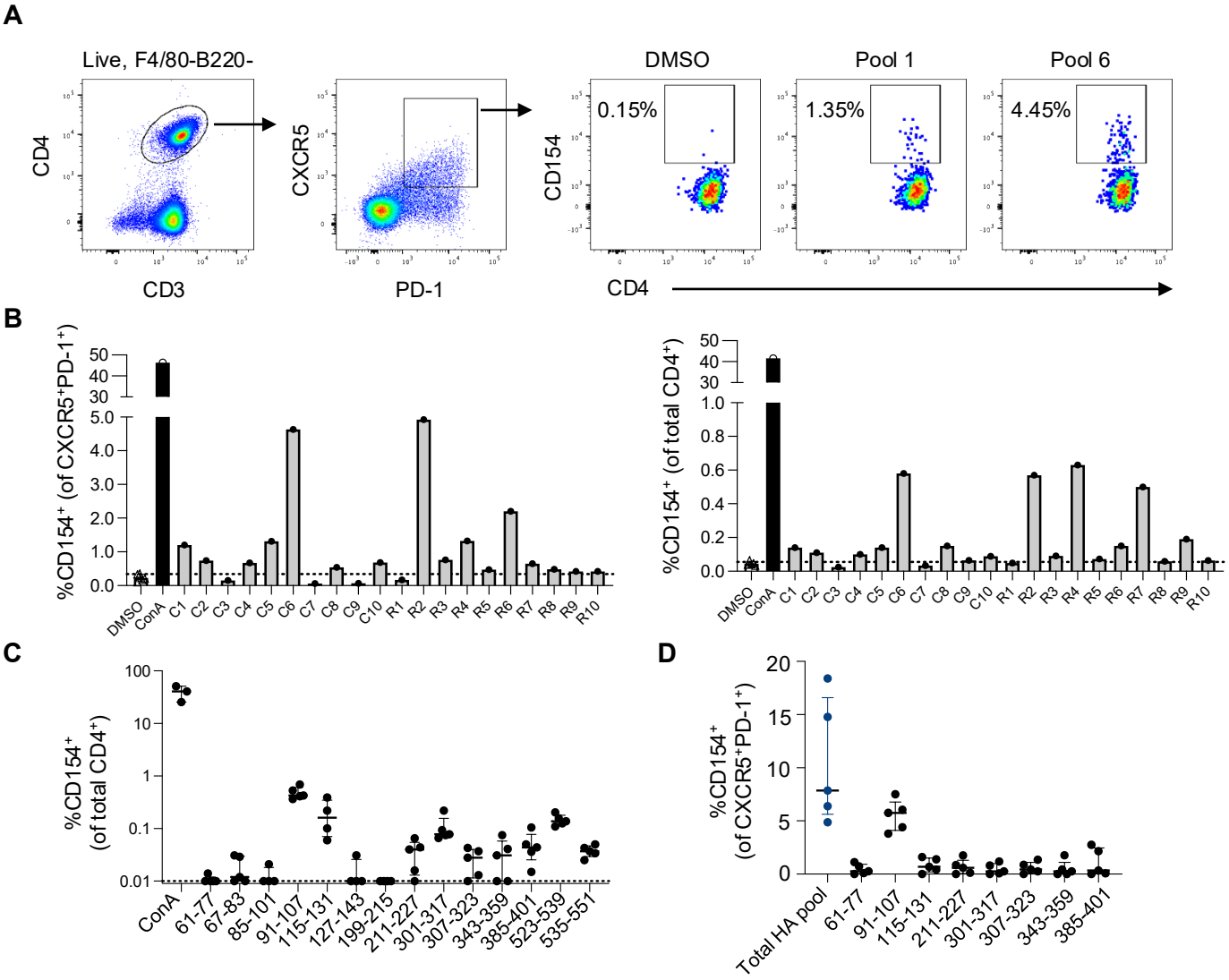

Supplementary Figure 3. Identification of immunogenic peptides in PR8 HA. (A) Representative staining of CD154 upregulation on CXCR5⁺PD-1⁺ CD4⁺ T cells in response to *in vitro* stimulation with peptide pools covering the PR8 HA protein. **(B)** Frequencies of peptide-specific or ConA-responsive cells among CXCR5⁺ (left) or total (right) CD4 T cells following PR8 infection. Each dot represents a single mouse (n=4-5 per group). **(C)** Frequencies of peptide-specific bulk CD4⁺ T cell responses in the mediastinal LN at day 35 post-PR8 infection. **(D)** Peptide- or pool-specific TFH responses in draining LN following intramuscular vaccination with soluble PR8 HA antigen.

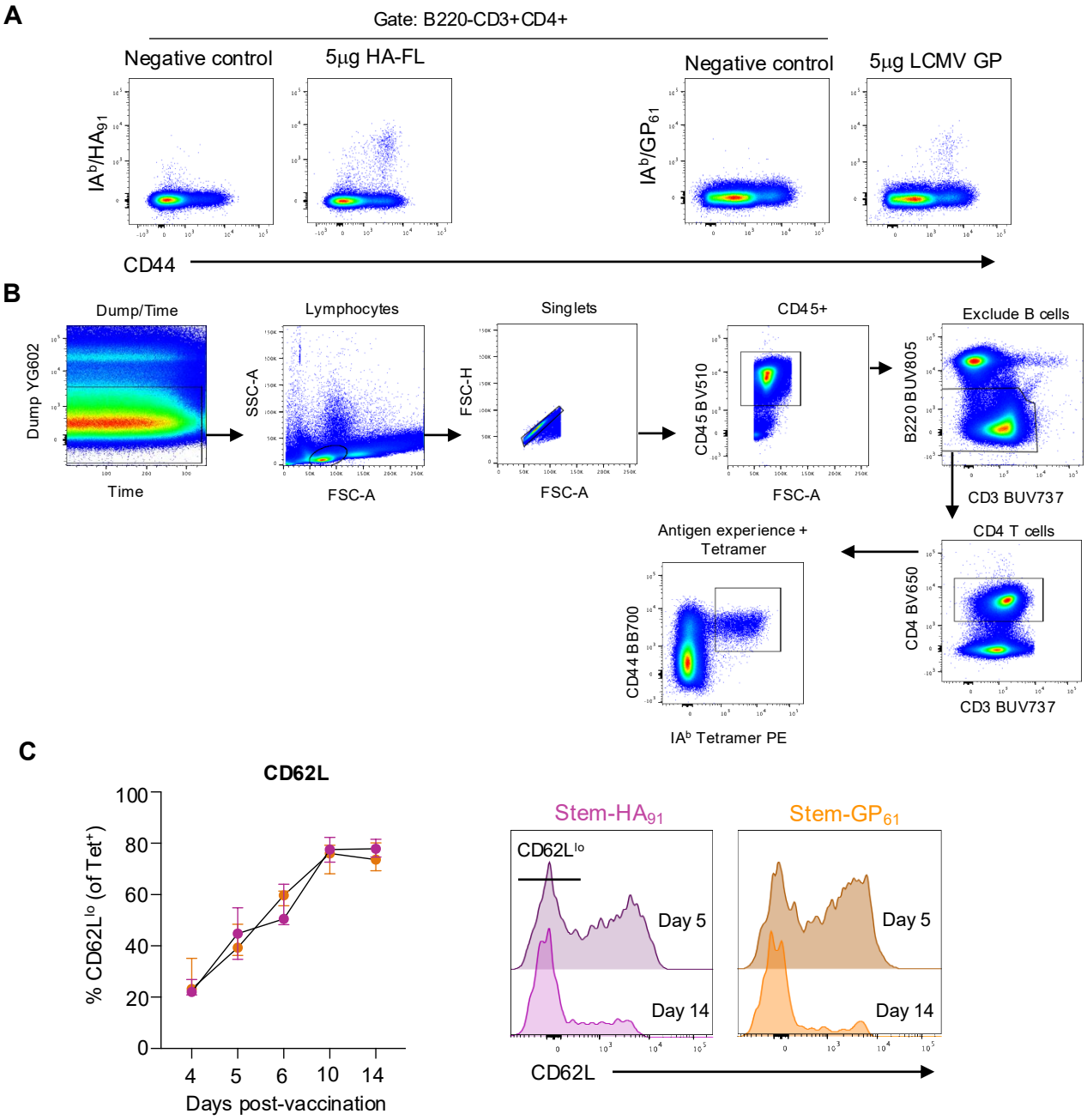

Supplementary Figure 4. Gating strategy for longitudinal tracking of antigen-specific CD4⁺ T cells. (A) Representative staining of IA^b/HA$_{91}$ and IA^b/GP$_{61}$ tetramers in draining lymph nodes at day 14 following HA-FL vaccination, PR8 infection or LCMV GP vaccination. **(B)** Antigen-specific cells were defined as Live, F4/80-CD45+B220-CD3+CD4+CD44hi tetramer+ lymphocytes. **(C)** Expression of CD62L on Tet⁺ cells from days 4-14 post-vaccination. Graph indicates median and IQR, N=5 per group.